

# Mechanisms beyond energetics revealed by multiscale kinetic modeling of 2D-material growth and nanocatalysis

Huijun Jiang | Zhonghuai Hou 

Hefei National Laboratory for Physical Sciences at the Microscale & Department of Chemical Physics, iChEM, University of Science and Technology of China, Hefei, China

## Correspondence

Zhonghuai Hou, Hefei National Laboratory for Physical Sciences at the Microscale & Department of Chemical Physics, iChEM, University of Science and Technology of China, Hefei, China.  
Email: hzhj@ustc.edu.cn

## Funding information

the Fundamental Research Funds for the Central Universities; Anhui Initiative in Quantum Information Technologies, Grant/Award Number: AHY090000; Ministry of Science and Technology of the People's Republic of China, Grant/Award Numbers: 2016YFA0400904, 2018YFA0208702; National Natural Science Foundation of China, Grant/Award Numbers: 21521001, 21673212, 21790350, 21833007, 21973085

**Edited by:** Jinlong Yang, Associate Editor.

## Abstract

Entanglement of spatial and/or temporal scales proposes great challenges to unravel mechanisms of complex chemical systems for their rational design. Multiscale modeling and calculations combining theoretical methods and algorithms at different scales provide powerful tools to address such problems. It has been conventionally known that energetics such as the reaction barrier plays an essential role in complex systems involving chemical reactions, in this review, we focus on recent progress of mechanisms beyond energetics revealed by multiscale kinetic modeling to emphasize the variety of underlying mechanism for such systems, and highlights the importance of kinetics in multiscale modeling and calculations for practical applications. Several interesting mechanisms as well as the corresponding concepts of multiscale kinetic modeling are described in detail, ranging from effects of geometry, micro-orientation, or reactant flux on 2D material epitaxial growth, to diffusion, directional mass transfer, or confinement enhanced electrocatalysis on nanocatalysts.

This article is categorized under:

Theoretical and Physical Chemistry > Reaction Dynamics and Kinetics

## KEYWORDS

2D-material growth, kinetic modeling, mechanism, multiscale simulation, nanocatalysis

## 1 | INTRODUCTION

For real world chemical systems, their behaviors may involve both the internal properties and external processes in surroundings at different spatial and/or temporal scales. The complexity of entangled scales ranging from sub-atomic level to mesoscopic even macroscopic level proposes great challenges to uncover the underlying mechanism of such systems, which further hinders rational design of man-made chemical systems with desired functions. For decades, researchers have made great efforts in developing multiscale calculation and modeling methods to tackle such challenges. Successful multiscale kinetic modeling has led to impressive deep insights in many complex chemical systems such as molecular self-assembly and polymer aggregation where weak interactions between molecules dominate.<sup>1-3</sup>

For chemical systems where chemical reactions are coupled with kinetics, nevertheless, the importance of kinetics has not been fully appreciated, even though it is well known that the overall performance of a chemical reaction is controlled by both the energetics and kinetics. This may be due to a conventional common sense that kinetics such as mass

transfer can always be easily accelerated enough in comparison with lowering the energetic reaction barrier, so that the coupling between reactions and other involved kinetic processes can be decoupled. However, such approximation may not be applicable when the characteristic size of the chemical system is comparable with that for the kinetics. For example, when electrocatalysts downsize to nanoscale, mass transfer deviates from the prediction by conventional theories<sup>4-11</sup> and should also be an elementary factor for performance of electrocatalysis at nanoscale.<sup>12-15</sup> Besides of nanocatalytic systems, another important type of chemical systems where kinetics may play an essential role is the epitaxial growth of 2D-materials on surfaces by chemical vapor decomposition.<sup>16</sup> As chemical resources are continuously supplied, the growth process is intrinsically out of equilibrium, making the grown materials also depending on the detailed growth pathways not only on the thermodynamic stability. The complicated coupling between reaction network and kinetics proposes great challenges for theoretical understanding of such chemical systems. As a result, even though 2D-material growth and nanocatalysis are two of the most important chemical systems attracting explosive researching attentions, so far, most of the theoretical understanding for such complex chemical systems only focus on the energetics by first principles calculations. It thus demands multiscale modeling and calculation for these complex chemical systems to investigate reactions coupled with kinetics.

In recent years, fortunately, several interesting mechanisms other than energetics have been revealed by establishing multiscale models and calculation methods to be able to include directly the kinetics. In this review, we first provide a brief review of the calculation methods relevant to different scales to facilitate ones familiar with them quickly. After that, we focus on recent progress of mechanisms beyond energetics revealed by multiscale kinetic modeling of 2D-material growth and nanocatalysis. This review aims to emphasize the variety of underlying mechanisms for complex chemical systems of reactions coupled with kinetics, and in turn highlights the importance of kinetics in multiscale modeling and calculations for practical applications.

## 2 | CALCULATION METHODS FOR COMPLEX CHEMICAL SYSTEMS

As mentioned above, the central issue for multiscale calculation of complex chemical systems is how to handle interactions and movements at different scales. So far, it is still unrealistic to build up a uniform multiscale calculation method explicitly including all the spatial and temporal scales simultaneously. Alternatively, an applicable way is to focus on a main scale depending on the special problem and system we are interested in, while other scales are coarse-grained to maintain their key physics. In practice, multiscale calculations may adopt a combination of calculation methods relevant to several given scales. For facility, we will bring a brief overview of some commonly used theoretical techniques and methods, including density functional theory (DFT), molecular dynamics (MD, classic or hybrid methods of quantum-mechanics/molecular-mechanics [QM/MM] MD), kinetic Monte-Carlo (KMC) simulation and continuum equations. Details about these techniques and methods can be found in many good reviews and books.<sup>17-36</sup> As we aim to review the progress of mechanisms beyond energetics for 2D-material growth and nanocatalysis, the most relevant theoretical techniques and methods are KMC and continuum equations, while DFT and MD provide the microscale information such as the reaction barrier or transition probability of kinetic events. Interestingly, the spirit of multiscale calculations, that is, the approximation of coarse-graining “less-relevant” degrees of freedom, also runs through nearly all of these methods for given scales themselves.

### 2.1 | Density functional theory

Basically, all of the observable properties for complex chemical systems are covered by quantum mechanics, which should be obtained directly from solutions of the corresponding Schrödinger equation for the motion of electrons and nuclei. However, exact solutions of the many-body Schrödinger equation with all degrees of freedom of a complex system are essentially difficult to be obtained. As an approximation, DFT based on functional of the spatially dependent electron density is proposed, where the electronic structure of the system is evaluated by applying effective potentials determined by the structure of the system and inter-electronic interactions on electrons.<sup>17-20</sup> DFT allows one to calculate the energy of the system and the forces acting on atoms without any empirical information input. Its calculation efficiency and sufficient chemical accuracy make DFT to be one of the most popular calculation methods at the atomic scale where the electronic structure is the main concern such as calculation of bond dissociation energies and corresponding activation barriers.

## 2.2 | Molecular dynamics

When the spatial and time scales increase to be ones where long-time movements of large number of atoms and molecules are important, DFT methods become computationally expensive to explicitly calculate interactions among them. Instead, classical MD simulations adopt empirical force-field potentials to describe implicitly the electronic-structure-induced interactions, by which forces acting on atoms and molecules are directly calculated and consequently the positions are updated according to Newton's equations.<sup>23-25</sup> The numerically solved trajectories of atoms and molecules can further be used to determine thermodynamic properties of the system with certain thermodynamic ensembles such as isothermal-isobaric ensembles (with constant number of particles, constant pressure, and constant temperature) or canonical ensembles (with constant number of particles, constant volume, and constant temperature). MD simulations explore the dynamics of atomic-level phenomena that cannot be observed directly in experiments, which have been widely applied in many fields to provide insights for, such as motion of macromolecules, structure and folding of proteins, deformation of materials, and so on.<sup>21-23,37</sup> Moreover, MD simulations are also able to investigate the effects of formation and breaking of chemical bond by using bond-order-based force-field potential.<sup>38,39</sup> Classical MD simulations are much faster and more computationally efficient than DFT calculations, however, the effective potentials governing the atomic interactions hold the key of accuracy for this method. Hybrid methods of QM/MM MD combine the advantages of classical and quantum methods to describe complex chemical systems. The basic idea of QM/MM is that, quantum methods are applied to ensure the accuracy for the core region of the system where chemical processes of interests take place, while other surrounding parts of large number of atoms and molecules are calculated by classical MD to obtain computational efficiency.<sup>40-45</sup>

## 2.3 | KMC simulations

MD describes all of the detailed movements of atoms and molecules on the potential energy surface of the complex chemical systems. However, for scales that chemical kinetics of the whole complex systems is focused, ones are usually not interested in such fast movements MD spend most of its time on, but in chemical events of slow jumps between different minima separated by energy barriers on the potential energy surface. KMC simulations model the system's kinetics by determining sequence of consecutive slow chemical events with realistic physical time while the fast movements of atoms and molecules are taken into account by stochastic transition probabilities for the events.<sup>26-30</sup> Combining KMC with other calculation methods is a powerful tool for multiscale simulations of complex chemical systems. For example, KMC with input transition probabilities calculated by DFT may bridge the gap between electronic structure and chemical kinetics. Analogue to the concept of QM/MM, combination of KMC focusing on a central region and continuum equations for others may facilitate computations of chemical engineering at nanoscales.

There are mainly two types of KMC algorithms, namely null-event algorithms and event-list algorithms. Given the transition probabilities of chemical events (which may be derived from DFT or MD calculations or from experimental data), null-event KMC samples the system's kinetics with a constant time scale by accepting or rejecting a candidate chemical event corresponding to the transition probabilities.<sup>46-48</sup> The null-event KMC is easy to be handled as the time-consuming and coding-complicated updating of all chemical events of the system is not necessary. However, it is quite inefficient if there are many trial events rejected. A general calculation procedure of the null-event KMC is as follows.

Step 1: Initialize the system.

Step 2: Randomly pick up a possible chemical event for the system.

Step 3: Estimate whether the selected event is allowed (a null event) depending on the current state of the system.

Step 4: If it is a null event, go back to Step 2.

Step 5: Update the state of the system according to the selected event.

Step 6: Go back to Step 2 till some termination conditions are fulfilled.

Event-list KMC, on the other hand, determines dynamically the next chemical event and the time step for its occurring based on a complete list of all events for current state of the system.<sup>49,50</sup> As there is certainly one chemical event happening for each step, the simulated time steps are usually larger than ones in null-event KMC, which thus accelerates the simulation process. In practice, the main challenge of the event-list KMC is that whether all the events can be identified for a given state. The algorithm of event-list KMC consists of following steps.

Step 1: Initialize the system.

Step 2: Update the list of all chemical events allowed by the current state of the system, as well as their associated rates  $r_i$ ,  $i = 1, \dots, M$ , where  $M$  is the total number of all events.

Step 3: Calculate the cumulative function  $R_i = \sum_{j=1}^i r_j$ .

Step 4: Generate a uniform random number  $u_1$  and update the time by a time step  $\Delta t = \ln\left(\frac{1}{u_1}\right)/R_M$ .

Step 5: Generate a uniform random number  $u_2$  and update the system state by event  $i$  fulfilling  $R_{i-1} < u_2 R_M \leq R_i$ .

Step 6: Go back to Step 2 till some termination conditions are fulfilled.

## 2.4 | Continuum equations

For scales much larger than that for each chemical event, the essentially discrete KMC methods become inefficient in simulation of chemical kinetics of the whole complex systems, too. As in such scales the number of molecules for chemical species as well as its change are large enough, it is then convenient to describe the system's kinetics by continuum equations mainly focusing on temporally (for well-mixed systems) or spatiotemporally (for spatially extended systems) continuous and differentiable mass densities of chemical species.<sup>31-36,51</sup> Other continuous quantities such as energy and momentum can also be included if necessary. Depending on the intensity of fluctuations, continuum equations may be formulated in the form of stochastic (for mesoscopic systems) or deterministic (for macroscopic systems) partial differential equations derived from basic physical principles such as the conservation of mass, energy or momentum, or by coarse-graining degrees of freedom below the scale of interest. Continuum equations are able to efficiently simulate mesoscopic or macroscopic systems for very long physical time, facilitating ones systematically investigate full kinetics of complex chemical systems to identify the key factors for functions of interest. A major disadvantage of continuum equations is that they are explicitly independent on atomic properties. However, if the continuum equations can be directly derived from the atomic level or combined with DFT and/or KMC, there are still possibilities to capture micro-scale effects on the macroscale behaviors.

A commonly used continuum equation for chemical systems is the reaction–diffusion equation consisting of reactions and normal mass diffusion due to concentration gradient, which reads

$$\frac{\partial c_i}{\partial t} = \sum_{j=1}^M f_{ij}(\{c_i\}) + D_i \nabla^2 c_i, i = 1, \dots, N,$$

where  $N$  is the total number of chemical species,  $M$  is the total number of reactions,  $c_i$  is the concentration of the  $i$ -th species,  $f_{ij}$  is the concentration change of the  $i$ -th species due to the  $j$ -th reaction, and  $D_i$  is the diffusion constant of the  $i$ -th species. Simulation of systems described by continuum equations usually involves numerical solving partial differential equations, for which many standard techniques can be adopted such as Euler's method or Runge–Kutta.

## 3 | MECHANISMS BEYOND ENERGETICS BY MULTISCALE KINETIC MODELING

In this part, some mechanisms beyond energetics for complex chemical systems revealed by multiscale kinetic modeling and calculation are reviewed. It is known that the energetic barrier is the most essentially decisive factor for reactions in simple chemical systems. However, when other scales of kinetic processes involve in complex systems, there may be chances for these kinetic processes to determine the reaction mechanisms. As two typical complex chemical systems, epitaxial growth of 2D materials and electrocatalytic reactions on nanocatalysts are mainly focused on.

### 3.1 | Geometry of graphene-substrate lattice mismatch determined epitaxial growth

Epitaxial growth of 2D materials is able to produce large scale 2D materials with high quality.<sup>52-54</sup> It has long been established that the reactant-substrate molecular interaction is essential for heterogeneous catalysis. However, the same quantic growth function of carbon monomer concentration was reported on both Ru(0001) and Ir(111) along the main growth orientation R0, while a different growth behavior from the main orientation was observed along another orientation R30 on the same Ir(111) surface.<sup>55,56</sup> The interesting similar growth kinetics on different substrates and different

growth kinetics on the same substrate imply a common growth mechanism independent on the specific carbon-metal interactions.

To address such a mechanistic issue, a multiscale calculation combining DFT and KMC methods were proposed.<sup>57</sup> Extensive DFT calculations were first performed to investigate all of the detailed chemical processes happening during the epitaxial growth of graphene on Ir(111) surface along the R0 orientation. By calculating the potential energy, diffusion barriers and attachment energy to the graphene edge for the most stable structures of surface carbon species, an inhomogeneous growth picture was revealed (Figure 1(a)), that is, while most sites locating at hollows between substrate atoms are thermodynamically favorable for attachment of carbon monomers (which is the most abundant carbon species on surface), there are also some sites atop the substrate atoms very unfavorable for carbon monomers where the growth must proceed via cluster attachment.

With the data and inhomogeneous growth picture revealed by DFT calculations, it still demands a mesoscopic calculation to directly simulate the growth behavior. As it aims to reveal the growth process with information at the atomic level, KMC calculation is a good choice. However, the KMC calculation of the epitaxial growth of graphene is not straightforward as a result of the following two main difficulties, that is, a huge unit cell is required to get statistically reliable growth due to the moving growth front, and the large disparate time scales needs to be included for different surface species due to their large density differences (e.g., the gap between densities of carbon monomers and clusters of five carbon atoms is about  $10^{15}$ ). As illustrated in Figure 1(b), a multiscale “standing-on-front” KMC model was proposed to overcome these difficulties. Based on the different dominant chemical processes, the model divides the whole surface into four regions. Contributions of the quasi-equilibrium distribution of carbon species in the far field and diffusions across the diffusion layer are compacted into effective carbon flux to the growth front, so that KMC calculation can focus the attachment and detachment processes of carbon species on the growth front. Furthermore, a multiscale KMC algorithm was designed to handle disparate time scales for different surface species. By grouping the KMC events by time scales of the relevant carbon species, a standard “event-list” KMC algorithm runs with groups of all time scales together. The group of the fast time scale in present simulation will be ruled out if graphene front gets stuck, so that the simulation can run automatically with the left slow time scales. The jump may keep to other slow time scales until the front moves again, after which all of the ruled out groups are included again in the simulation. The detail procedure of the algorithm is as follows.

Step 1. Initialize the system, and group all KMC events by their time scales.

Step 2. Run a standard event-list KMC algorithm with present groups of events (i.e., Step 2–6 in the procedure of event-list KMC described in the part of calculation methods for complex chemical systems).

Step 3. If the graphene front gets stuck, rule out the group of events with the fast time scale in present simulation, by which the simulation will automatically jump into the next slow time scale.

Step 4. Go back to Step 2 till the graphene front grows again.

Step 5. Include again all of the groups and go back to Step 2 till some termination conditions are fulfilled.

With all atomic parameters estimated by DFT, the KMC obtained a dependence of growth rate on the surface carbon monomer concentration with an exponent of 5.25, reproducing well observations in experiments.<sup>57</sup> Detailed analysis of the key KMC events revealed that, though carbon monomers dominate attachment over thermodynamically favorable hollow sites, only large clusters with more than five carbon atoms can contribute neatly to the front growth over thermodynamically unfavorable atop sites. As plotted in the inset in Figure 1(c), the reason is simply that only clusters with more than five carbon atoms can complete and stabilize the growth front due to the lattice-mismatch between graphene and the substrate.<sup>58</sup> Remarkably, the growth exponent saturates to a constant value slightly larger than 5 when the effective carbon-substrate interaction strength passes over a threshold, indicating a robust growth mechanism solely determined by the geometry of lattice-mismatch between graphene and the substrate.<sup>58</sup> Such a geometry-determined growth mechanism was further verified by applying the above KMC calculation on growth over R30 on Ir(111) surface. Similarly, the growth exponent is robust, too, if the carbon-substrate interaction is strong enough, which is about 2 determined by the sparse distribution of atop sites along this orientation (Figure 1(d)). The geometry-determined mechanism of graphene growth explains why similar kinetics have been observed in experiments for different substrates and different kinetics for different orientations on the same substrate.

The theoretically revealed effect of lattice mismatch between graphene and the metal substrate on the growth of graphene was then confirmed by experiments about kinetics of graphene formation on Rh(111) investigated by in situ scanning tunneling microscopy.<sup>59</sup> Interestingly, the experiments also present new challenges for simulations of graphene growth kinetics. As the aforementioned “standing-on-front” KMC simulation is actually a quasi-1D calculation method, it is still not applicable for some growth behaviors have to be calculated by fully 2D methods. For example,

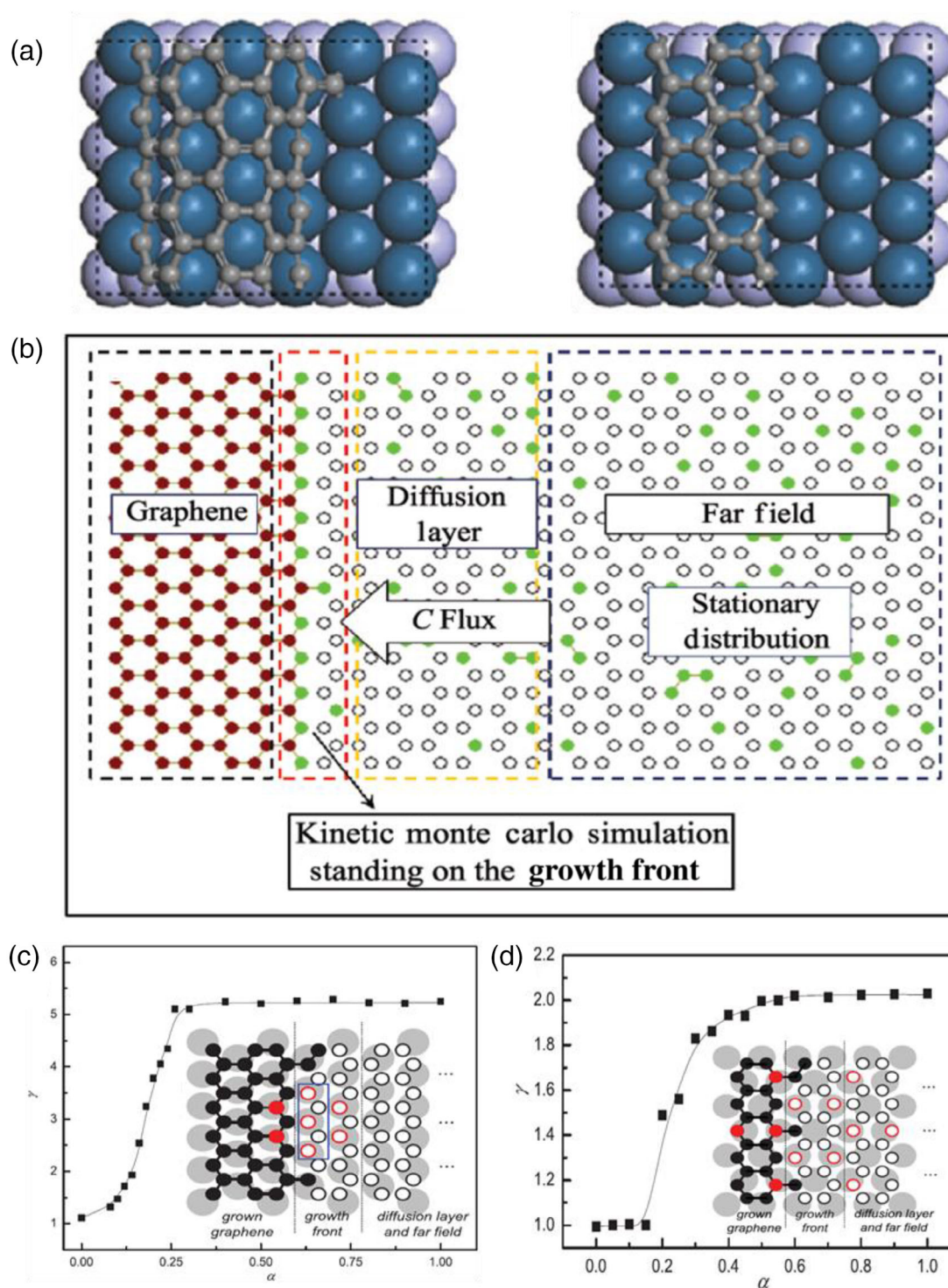


**FIGURE 1** (a) Heterogeneous growth of carbon monomers on a zigzag Ir R0 ribbon. The attachment is thermodynamically favorable to occupy a top site (the left panel) and unfavorable to occupy a hollow one (the right panel). (b) Schematic diagram of the KMC model standing on the graphene growth front. The dependence of growth exponent  $\gamma$  on effective carbon-substrate interaction strength  $\alpha$  for (c) R0 and (d) R30 orientation. Insets show the lattice-mismatch for R0 and R30, respectively. (Figure adapted with permissions from References 57 and 58. Copyright 2012 American Chemical Society and 2013 American Physics Society)

experiments in Reference 59 observed time-resolved growth behaviors beyond conventional growths over the large scale of moiré patterns when several adjacent fragments merge into one whole piece of grown graphene. To explore large-scale graphene growth of fully 2D shapes, a coarse-grained KMC model was further established based on the above

multiscale calculation combining DFT and KMC methods, where only chemical events of net contribution to growth are maintained.<sup>60</sup> The coarse-grained KMC model facilitates simulation of graphene growth over surface of at least millions of sites, and revealed that the nonlinear time-resolved growth behaviors over vacancy islands inside the flake of graphene observed in experiments in Reference 59 is also a result of the geometry-determined growth mechanism.<sup>60</sup>

### 3.2 | Micro-orientations determined grain boundary formation mechanism

Beside of the epitaxial growth for one single grain, a realistic growth process may consist of multiple grains.<sup>61,62</sup> As a typical defect for systems with multigrain growth, formation of grain boundary strongly affects the mechanical, thermal, electric, or optical properties of 2D materials.<sup>63-66</sup> Therefore, a fundamental understanding of the formation mechanism for grain boundaries is demanded.

Specifically, grain boundary formation of monolayer MoS<sub>2</sub> was investigated by a KMC model combined with first-principles calculations.<sup>67</sup> The KMC model considered growth of two initial grains of equilateral triangle shape separately located with different micro-orientations (Figure 2(a)). Each grain grows up by the attachment of S and Mo adatoms along its own lattice structure. As the experimental growth is usually in sulfur-rich environment, the adjacent S vacancies will be quickly filled as soon as a Mo adatom attached. DFT calculated energetic barriers for adatoms attachment show that adatoms attached to a complete zigzag edge, that is, kink nucleation, is hard, after which consequent attachment, namely kink propagation, is much faster (Figure 2(b)). A grain boundary will be formed once two independent grains impinge and no more adatoms are able to fill in between the two grains.

With standard procedures as described in the part of calculation methods for complex chemical systems, the KMC simulations well reproduced experimental observations in refs. [61, 68, 69] with the same setup as in experiments. It was revealed that the overall growth orientation of the grain boundary exactly equals to the composition of kink propagation micro-orientations for the two approached edges (Figure 2(c)). What's more, the grain boundary roughness is determined by the difference between the micro-orientation angles of the two grains (Figure 2(d)). When the angle difference is small, a smooth grain boundary will be formed. On the contrary, a rough grain boundary will be observed when the difference is large. Therefore, this work actually found a micro-orientations determined grain boundary formation mechanism for the multigrain growth of MoS<sub>2</sub>.

### 3.3 | Reactant flux affected anisotropic growth of 2D transition metal dichalcogenide

Controllable anisotropic growth is another issue in synthesis of 2D materials for the fabrication of electronic and optoelectronic devices.<sup>70-72</sup> However, some typical 2D materials such as transition-metal dichalcogenides (TMDCs) tend to form isotropic nanoplates rather than anisotropic nanoribbons.<sup>73,74</sup> Understanding key factors for anisotropic growth then facilitates its controllable synthesis.<sup>75,76</sup>

As shown in Figure 3(a), anisotropic WS<sub>2</sub> nanoribbons were successfully fabricated by a space-confined and substrate-directed strategies combined with the chemical vapor deposition method.<sup>77</sup> In experiments, one piece of SiO<sub>2</sub>/Si substrate was placed at the center of furnace with tungsten trioxide powder randomly scattered on the substrate surface, and another piece of SiO<sub>2</sub>/Si substrate was put facedown above the bottom substrate forming a confined space. Sulfur powder was placed about 24–25 cm away from the central region of furnace. H<sub>2</sub>/Ar was used as the carrier gas with a fixed flow rate. It was found that the gap between two substrates provides a steady environment to precisely control the growth kinetics, so that the kinetic growth dominants to produce TMDC nanoribbons even though TMDC nanostructures are generally thermodynamic stable. To illustrate this effect clearly, a computational fluid dynamics method is performed using a commercial computational fluid dynamics software package (CFD-ACE 2008, ESI) to simulate the flow field and velocity distribution of gas flux in the tube and confined space at the mesoscopic scale. While calculated flux velocities vary largely at different locations outside the confined space, ones in the confined space are much slower and stable, validating the conclusion in experiments (Figure 3(b)).

In another theoretical work, a KMC model combining DFT calculations was proposed to understand the growth kinetics at the atomic level.<sup>78</sup> The model aims to simulate the anisotropic growth of monolayer WS<sub>2</sub> on ST-X quartz by the chemical vapor deposition method. Essential kinetic events concerned in the growth process, such as adsorption, desorption, and diffusion, are included and simulated by standard KMC procedures. KMC calculations showed that chalcogen/metal ratio determined by the reactant flux at the mesoscopic scale contributes mainly to the anisotropic growth of WS<sub>2</sub>. As

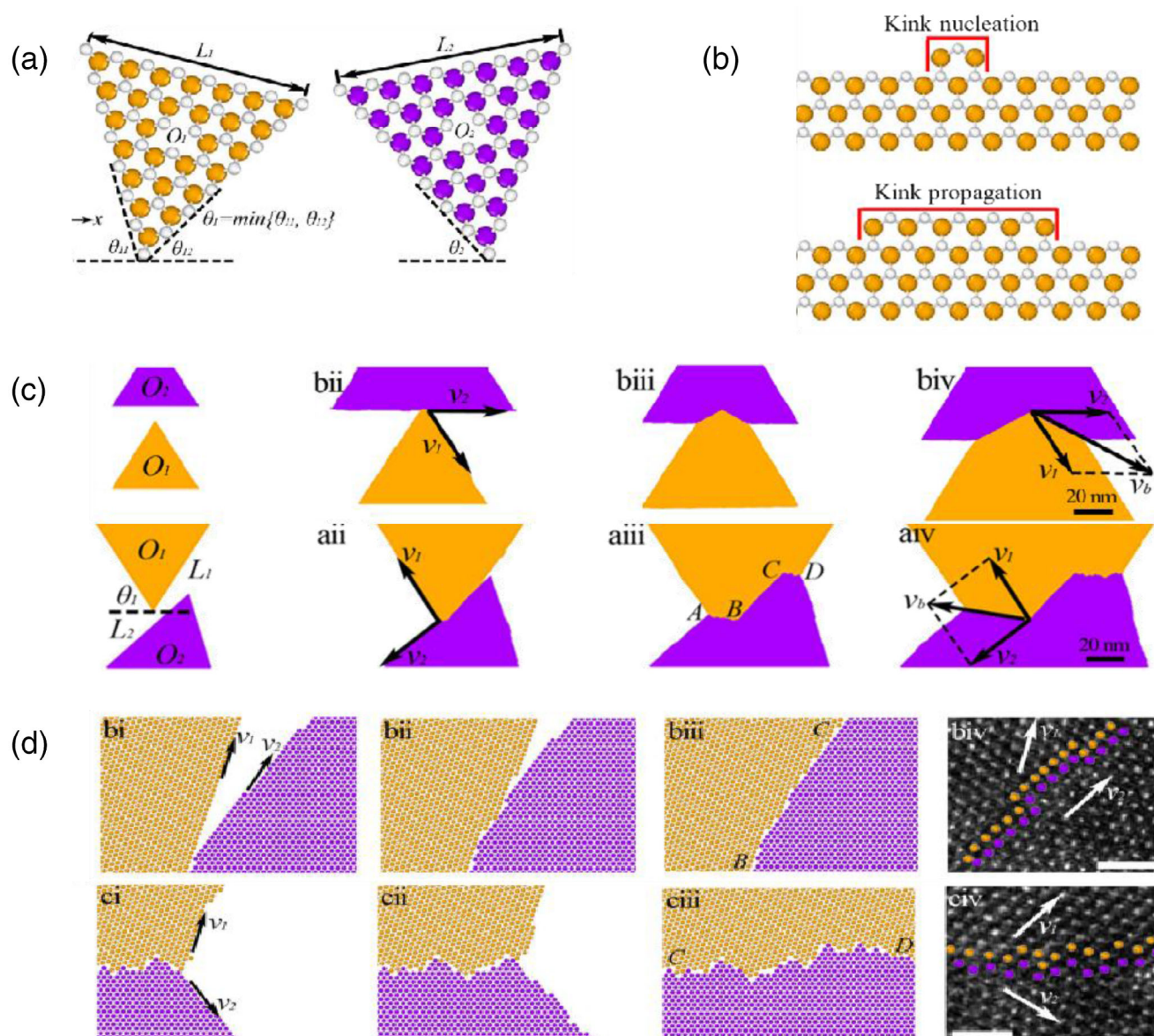


**FIGURE 2** (a) Schematic of MoS<sub>2</sub> grain growth model. (b) Kink nucleation and propagation at a MoS<sub>2</sub> zigzag edge. (c) Grain boundary formation in KMC simulations. The overall growth orientation of the grain boundary ( $v_b$ ) is the composition of kink propagation vectors at the two edges ( $v_1$  and  $v_2$ ). (d) Formation kinetics of (bi–biii) smooth BC grain boundary and (ci–ciii) rough CD grain boundary during two-grain growth in KMC simulations. High-resolution STEM image of (biv) smooth and (civ) rough grain boundaries. Scale bars are 1 nm. (Figure adapted with permissions from Reference 67. Copyright 2019 American Chemical Society)

plotted in Figure 3 (c), an appropriate chalcogen/metal ratio window facilitates kinetic growth of anisotropic nanoribbons, while triangle flakes may form for smaller ratio and dendritic flakes for larger ratio. The KMC simulation at the atomic scale along with the above fluid dynamics calculations illustrates a reactant flux affected anisotropic growth of 2D TMDC.

### 3.4 | Diffusion-influenced electrochemical responses on nanoparticle-covered electrodes

Design of nanoscale electrocatalysts with desired selectivity and activity plays a significant role in energy conversion and environment preservation. When catalysts downsize to nanoscale, the mass transfer deviates from the prediction of conventional theories due to the comparability of length scales between the catalyst size and reaction region. The significance of mass transport on nanoscale may not be neglected for reactions on nanoscale electrocatalysts.

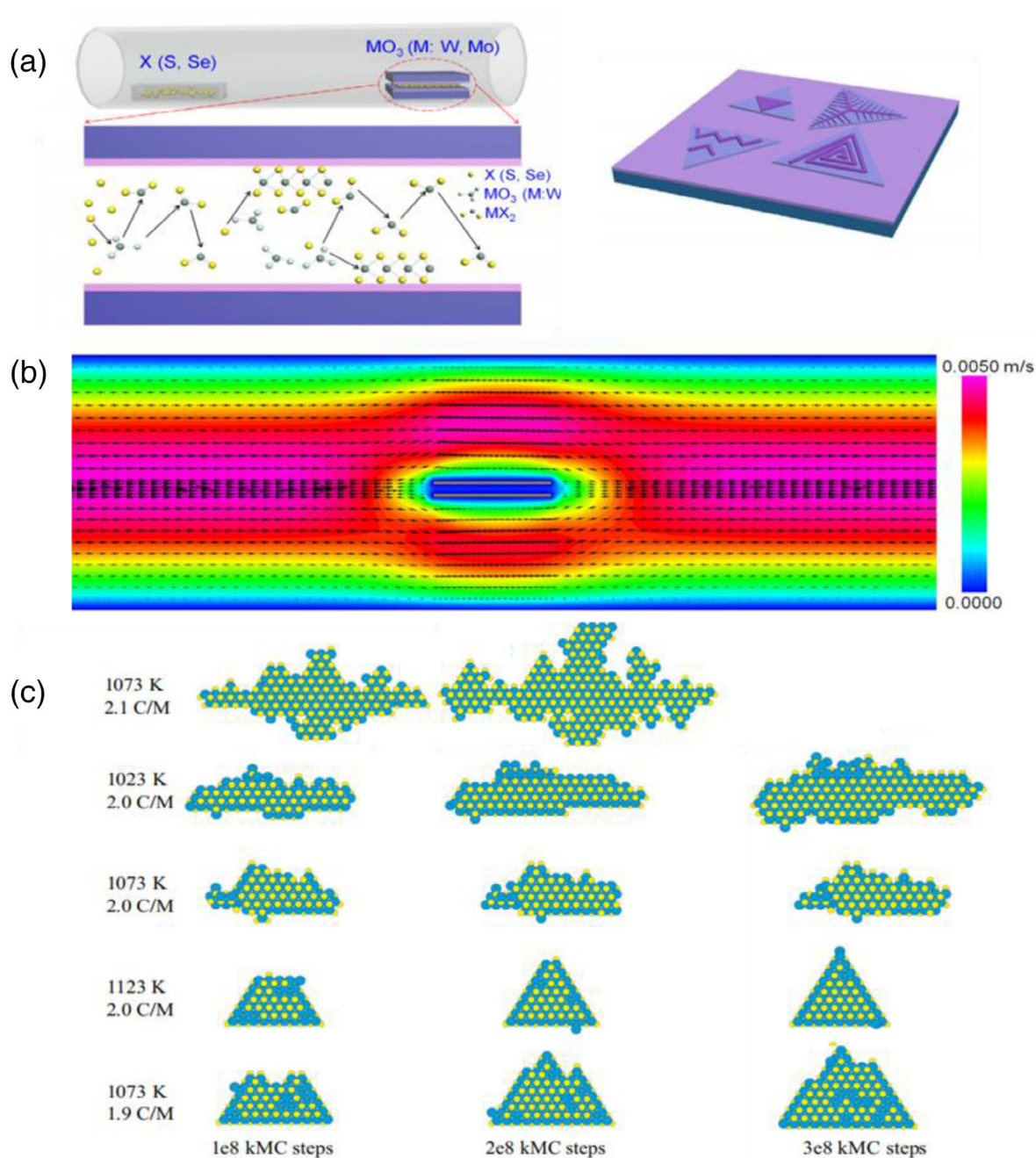


**FIGURE 3** (a) Schematic of controlled synthesis procedure for TMDC nanoribbons. (b) Flow field distribution within the tube and space-confined region. (c) The KMC simulated growth morphologies of monolayer  $WS_2$  under diverse experiment conditions. (Figure adapted from Reference 77 with permissions and from Reference 78 under the terms of the Creative Commons CC BY license for open access articles. Copyright 2020 Elsevier.)

To understand the effect of mass transport by diffusion at nanoscale, Compton and co-workers proposed a kinetic model of a nanoparticle on a planar electrode, where diffusion from bulk solution to the particle surface and electrocatalytic reactions are included<sup>10</sup> (the left panel in Figure 4(a)). Without loss of generality, continuum mass-transport equations were employed to describe diffusion of species with boundary conditions containing a simple electrochemical reaction  $A + ne^- \leftrightarrow B$  on the nanoparticle, as

$$\frac{\partial a}{\partial t} = \frac{\partial^2 a}{\partial R^2} + \frac{1}{R} \frac{\partial a}{\partial R} + \frac{\partial^2 a}{\partial Z^2}$$

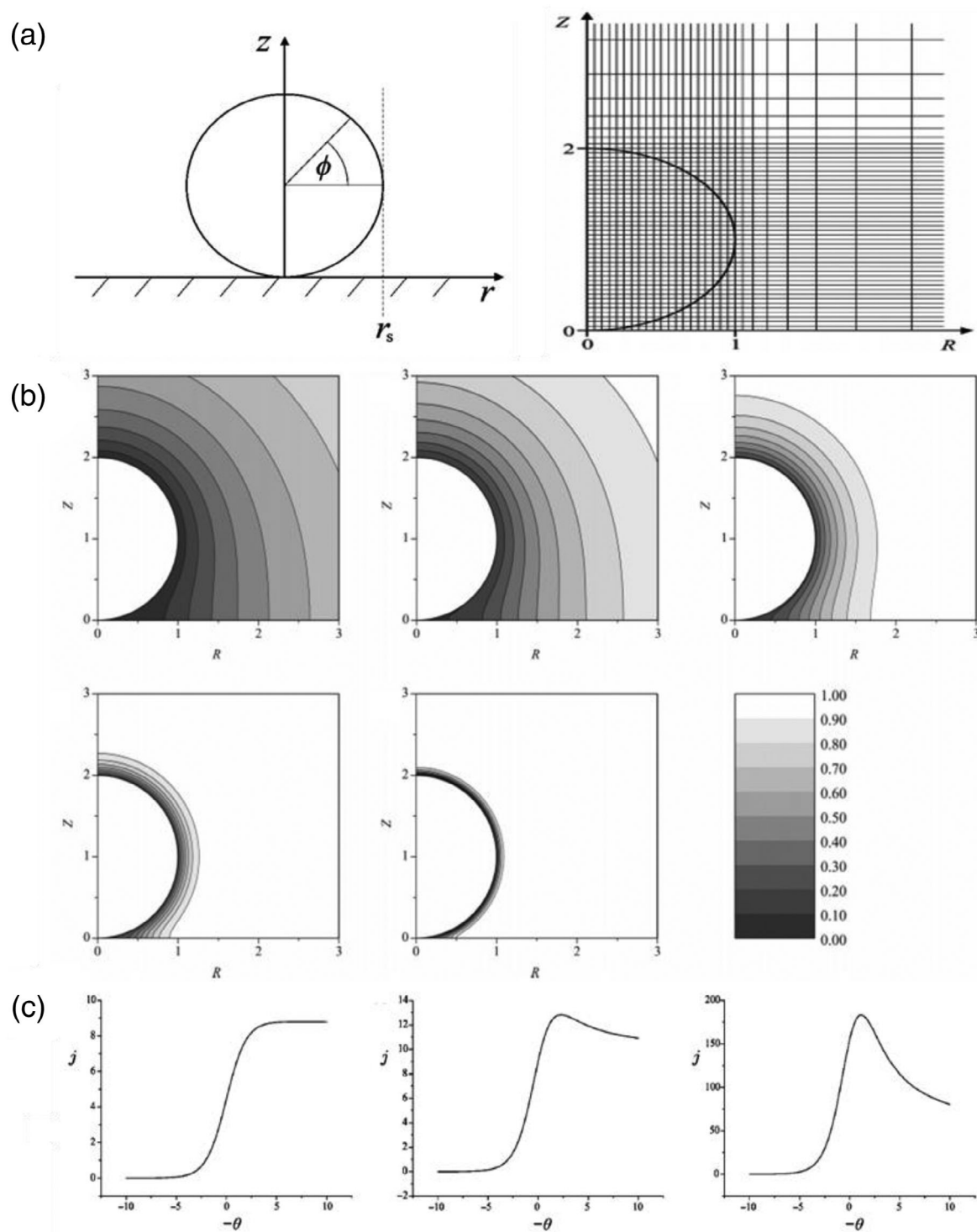


**FIGURE 4** (a) Schematic of a spherical particle sitting upon a supporting planar surface (left) and the grid used for discretization of the sphere (right). (b) Simulated concentration profile around the spherical particle at scan rate  $\delta = 0.1, 1, 10, 100, 1000$ , respectively. (c) Simulated voltammetry for a reversible electrode transfer at  $\delta = 0.001, 1, 1000$ , respectively. (Figure adapted with permissions from Reference 10. Copyright 2007 American Chemical Society)

where  $a$  is the normalized concentration of reactant  $A$ ,  $Z$  is the axial coordinate which is defined normal to the plane, and  $R$  is the cylindrical radial coordinate. By a specially designed discretization of the nanoparticle to be grids (the right panel in Figure 4(a)), the mass-transport equations are able to be solved in cylindrical polar coordinates, so that the

nanoscale diffusion can be related to the measured electric current in linear sweep voltammetry at the experimental scale.

In Figure 4(b), concentration profiles around the nanoparticle are plotted. A significant depletion of the reactant emerges when the sphere meets the supporting plane. The diffusion layer thickness is enlarged and then leads to larger reactant depletion region as the scan rate decreases. This diffusion-influenced concentration distribution further determined the overall electrochemical responses of the system as shown in Figure 4(c). When the scan rate varies from slow to fast, the flux density becomes uniform over the sphere surface as the reactant depletion region reduced with the decreased size of diffusion layer, revealing a diffusion-influenced electrochemical response for electrocatalysis on nanoparticles.

Compton et al. further studied the diffusion-influenced electrochemical responses of electrode covered by multiple catalytic nanoparticles with the same kinetic model.<sup>9</sup> They found that overlapped diffusion layer between adjacent particles would lead to several types of concentration distributions for different coverage of nanoparticles, which then result in various electrochemical responses. Besides, the influence of the nanoparticle size is also explored with this model.<sup>12</sup> Moreover, the kinetic model can also be applied to oxygen reduction reaction on a gold macroelectrode and on an electrodeposited gold nanoparticle modified glassy carbon electrode, where the mechanism of diffusion-influenced electrochemical response also works.<sup>79,80</sup>

### 3.5 | Local-field-induced mass transfer enhanced electrocatalytic performance

Besides of the mass transport due to normal diffusion, there may be directional mass transfer by emerged micro-interactions at the nanoscale. Recently, Liu et al. reported a fascinating yet simple strategy to enhance electrocatalytic reduction of CO<sub>2</sub> by placing catalytic tips of different curvature on Au electrode.<sup>14</sup> The reduction rate can be increased to be two orders of magnitude higher on needle type of catalysts (of diameter about 50 nm) than that on particle type ones (diameter about 500 nm) while the efficiency was enhanced up to 90%. It was observed experimentally that high curvature of catalysts can, on the one hand, lower the reaction barrier about 51 kJ/mol, on the other hand, increase the CO<sub>2</sub> concentration around catalysts by curvature induced local electric field. It is known from the Arrhenius equation that the reaction should be accelerated about seven orders of magnitude for such a decrease of the reaction barrier, which is much faster than the experimental observation. The large discrepancy thus indicates a mechanism other than lowering the reaction barrier for the sharp-tip enhanced electrocatalytic reduction of CO<sub>2</sub>.

Jiang, et al. then proposed a multiscale kinetic model and corresponding calculation method to reveal the underlying mechanism of the sharp-tip enhanced electrocatalytic reduction of CO<sub>2</sub>.<sup>15</sup> As shown in Figure 5(a), the model consists of a cell of one single catalytic tip with periodic boundary conditions. Main kinetics of the whole catalytic process is considered, including adsorption of CO<sub>2</sub> from solution to the electrode, diffusion over the surface, and reductions at the tip. Specially, as CO<sub>2</sub> molecules can be concentrated on the tip by curvature-induced local electric field, the conventional continuum reaction–diffusion equations were not applicable to the system. The reaction–diffusion equations taking the molecule-field interaction into account were derived from the system's free-energy density functional by dividing the surface into  $N \times N$  boxes inside each of which the total number of chemical molecules is large enough to ensure the definition of relevant thermodynamic quantities, and also small enough so that these quantities can be considered as constants. The system's free-energy density functional in box locating at  $\mathbf{r}$  with molecule-field interaction potential  $V(\mathbf{r})$  then reads

$$f(\mathbf{r}) = V(\mathbf{r}) + k_{\text{B}}T[\theta(\mathbf{r})\ln(\theta(\mathbf{r})) + (1-\theta(\mathbf{r}))\ln(1-\theta(\mathbf{r}))]$$

where  $k_{\text{B}}$  is the Boltzmann constant,  $T$  is the temperature,  $\theta$  is the surface concentration normalized by its maximal values. The chemical potential can be derived as

$$\mu(\mathbf{r}) = \frac{\partial f(\mathbf{r})}{\partial \theta} = \partial_{\theta}V(\mathbf{r}) + k_{\text{B}}T\ln\frac{\theta(\mathbf{r})}{1-\theta(\mathbf{r})}.$$

By assuming the transport process is not too far from equilibrium, the diffusion flux depends linearly on the corresponding driving force as

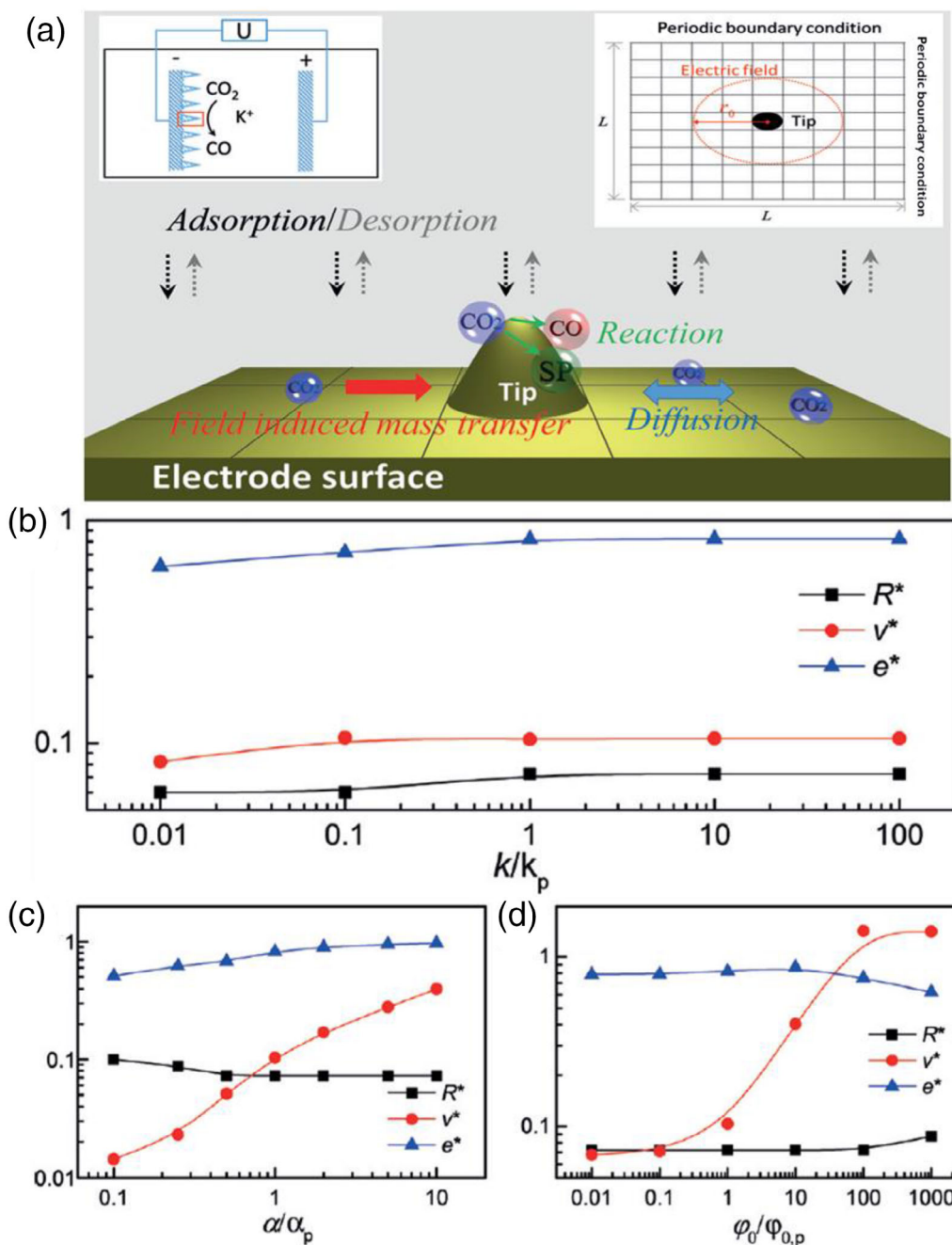


**FIGURE 5** (a) The kinetic model for electrocatalytic reduction of CO<sub>2</sub> near a tip on electrode surface. SP denotes side products rather than CO. Insets show the experimental setup in Reference 14 (top left) and the numerical simulation setup (top right). Optimal performance depending on (b) the energetic barrier, (c) the interaction strength between adsorbed CO<sub>2</sub> and the locally induced electric field, and (d) the effective adsorption rate for CO<sub>2</sub> on the electrode surface. Where  $R^*$ ,  $v^*$ , and  $e^*$  are the tip size, CO producing rate, and efficiency when the optimal performance is achieved. (Figure adapted with permission from Reference 15. Copyright 2017 John Wiley and Sons)

$$J(\mathbf{r}) = -L\nabla\mu(\mathbf{r}) = -L\left[\nabla(\partial_\theta V) + \frac{k_B T}{\theta(\mathbf{r})(1-\theta(\mathbf{r}))}\nabla\theta(\mathbf{r})\right],$$

which should back to Fick's law if  $V(\mathbf{r})$  is absent. Thus,  $L = [D\theta(\mathbf{r})(1-\theta(\mathbf{r}))]/k_B T$  can be derived, and eventually the reaction–diffusion equations with molecule–field interaction read

$$\begin{aligned}
 \frac{\partial \theta(\mathbf{r})}{\partial t} &= \varphi_0(1-\theta) - k_d\theta - k\theta - k_s\theta + D\nabla^2\theta \\
 &\quad - \frac{D}{k_B T} \nabla \cdot [\theta(1-\theta)\nabla(\partial_\theta V)] \\
 \frac{\partial \theta_{co}(\mathbf{r})}{\partial t} &+ k\theta - k_d^{co}\theta_{co} + D_{co}\nabla^2\theta_{co} \cdot \\
 \frac{\partial \theta_{sp}(\mathbf{r})}{\partial t} &= k_s\theta - k_d^{sp}\theta_{sp} + D_{sp}\nabla^2\theta_{sp}
 \end{aligned}$$

Here,  $\varphi_0$ ,  $k_d$ ,  $k$ , and  $k_s$  are rate constants of the effective adsorption, desorption, reaction from CO<sub>2</sub> to CO, and the effective reaction to possible side products SP, respectively. The corresponding quantities with subscript “co” and “sp” are those for CO and SP.  $V$  is the interaction potential between CO<sub>2</sub> molecules and the local electric field.

With the proposed kinetic model and derived reaction–diffusion equations, numerical simulations showed that the energy barrier alone is not the decisive factor that controls the optimal overall reaction rate and efficiency (Figure 5(b)), implying that the reaction has already been accelerated enough so that the optimal sharp-tip enhanced performance cannot be further enhanced by simply lowering the energy barrier of the main reaction. Alternatively, the field-induced mass transfer on the surface and adsorption of the reagent to the surface were shown to be key factors (Figure 5(c), (d)), providing a kinetic view of the sharp-tip enhanced electrocatalytic reduction of CO<sub>2</sub> that when normal diffusion of CO<sub>2</sub> to the tip cannot match the fast reaction, the field-induced attraction can supply extra CO<sub>2</sub> to provide a better performance. The mechanism of local-field-induced mass transfer enhanced electrocatalytic performance implies possibility to boost electrocatalytic reaction on nanocatalysts besides of reducing the reaction barrier.

Soon after, well-designed nanocatalysts with periodic structures were demonstrated to be of abilities to enhance catalytic performance of the methanol oxidation reaction or formic acid oxidation reaction on catalytical nanowires, nanoparticles, nanorods, or nanoflakes.<sup>81</sup> Based on similar multiscale modeling and simulations, it was found that the enhancement stems from regulation of the surface reactant flux by the gradient of the local electric field directing uniformly to the nearest catalyst on ordered patterns, so that the kinetics was optimized to enrich the local concentration of reactant molecules for reactions. Furthermore, the mechanism has also been verified in electroreduction of CO<sub>2</sub> on high curvature transition metal chalcogenide nanostructures,<sup>82,83</sup> Cu@Bi nanocones,<sup>84</sup> sharp Cu@Sn nanocones on Cu foam,<sup>85</sup> Cu-based heterogeneous electrocatalysts,<sup>86</sup> sharp tipped zinc nanowires,<sup>87</sup> polytetrafluoroethylene protected copper nanoneedles,<sup>88</sup> fluorine doped cage-like carbon electrocatalysts,<sup>89</sup> nickel-nitrogen-modified porous carbon/carbon nanotube hybrid with necklace-like geometry,<sup>90</sup> as well as sharp-tip enhanced catalytic CO oxidation by atomically dispersed Pt1/Pt2 on a raised graphene oxide platform<sup>91</sup> and electrocatalytic hydrogen evolution on atomically dispersed platinum supported on curved carbon supports.<sup>92</sup>

### 3.6 | Confinement effect of electrode on the selectivity of desired production

Similar to the above, precisely controlled morphology of nanofabricated electrodes was reported to be an efficient strategy for systematically controlling the product selectivity and reaction kinetics of electrocatalytic reaction.<sup>93</sup> Catalysts with hollow or porous structures have been demonstrated as a specific morphology of ideal electrode to control the selectivity of higher-order carbon products (C<sub>2+</sub>) in electrocatalytic reduction of CO<sub>2</sub>/CO recently.<sup>93,94</sup>

Multiscale kinetic simulations combining DFT and continuum diffusion–reaction equations are employed to reveal the mechanism of confinement-enhanced selectivity of C<sub>2+</sub> feedstock at hollow-structured catalysts.<sup>95,96</sup> Energy landscape of C<sub>2+</sub> formation as well as its competing pathways such as H<sub>2</sub> or C<sub>1</sub> production was calculated by DFT, where C<sub>2</sub> is produced by CO dimerization and further couples with CO to be C<sub>3</sub> productions.<sup>95,97</sup> With reaction pathways and energetic parameters calculated by DFT, a more comprehensive kinetic model in terms of reaction–diffusion equations is employed focusing on the hollow-confined mass transfer effects.<sup>96</sup> As the reaction–diffusion equations are standard ones, they were solved by using the COMSOL Multiphysics software package.

Simulations of the kinetic model found that, the outflow of local produced C<sub>2</sub> species is restricted by the cavity of the hollow-structured catalyst, leading to higher C<sub>2</sub> intermediate concentration in the cavity. Consequently, desorption of C<sub>2</sub> will be reduced and ultimately generates a heightened C<sub>3</sub> production inside the cavity (Figure 6(a)). This kinetic model successfully reveals that the confinement effect of catalysts would regulate the flow of intermediate and further

modify the local concentration of intermediate to optimize the catalytic selectivity. Interestingly, it can also be obtained from the kinetic model that the open angle of the cavity influences the ratio of  $C_3/C_2$ . An optimized open angle for the highest selectivity of  $C_3/C_2$  can be derived with the simulation results, which agrees with the experimental data well (Figure 6(b)). This kinetic model, therefore, uncovers a mechanism of confinement-tuned selectivity for CO electrocatalytic reduction. This mechanism was further utilized to propose a multi-hollow structured catalyst which enhances the selectivity of  $C_{2+}$  product for electrocatalytic reduction of  $CO_2$ <sup>94</sup> (Figure 6(c); Box 1).

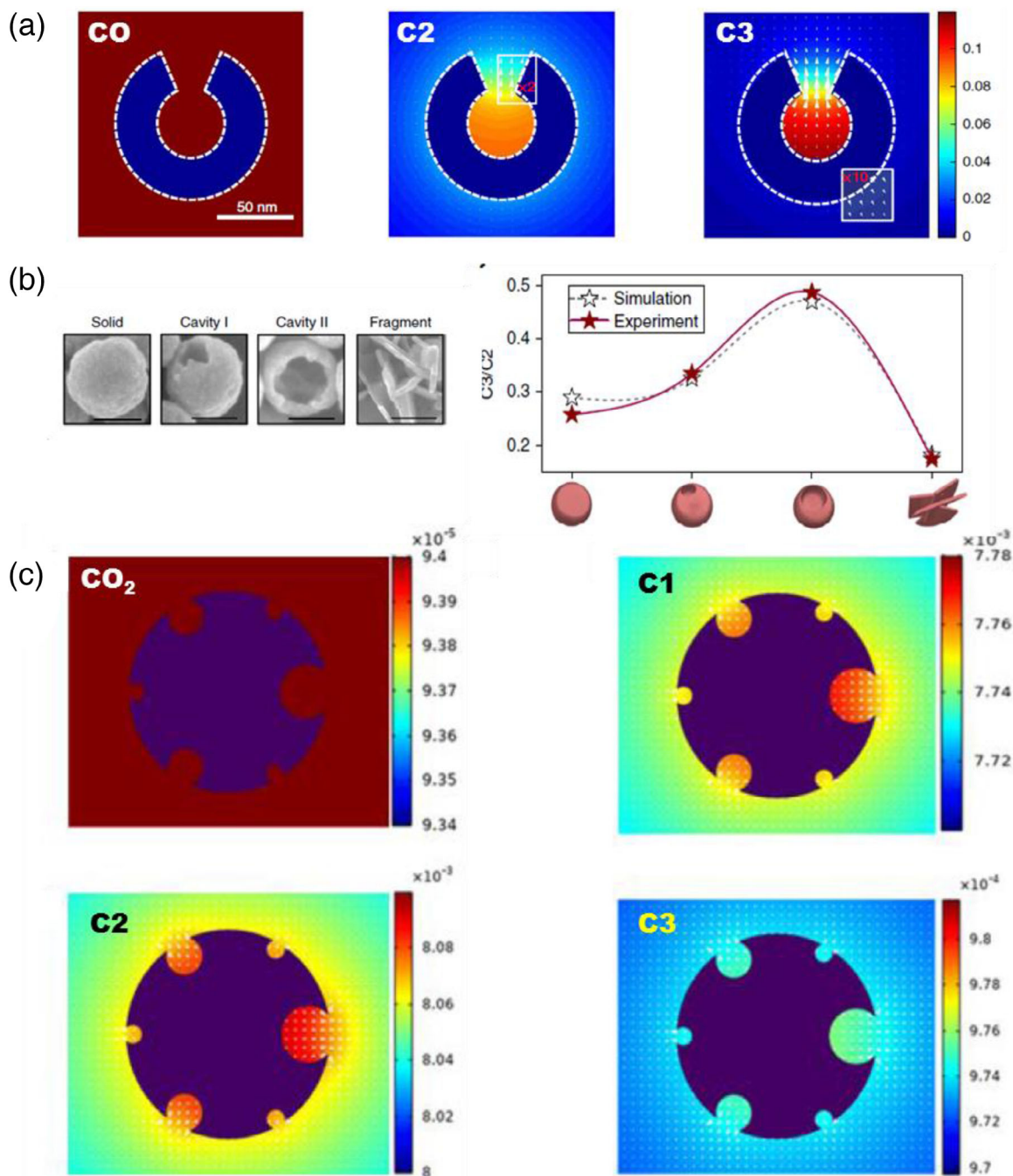


**FIGURE 6** (a) The concentration distributions of CO (left), C<sub>2</sub>(middle), C<sub>3</sub>(right). (b) The morphology structures of solid, cavity I, cavity II and fragment (left) in experiments. The simulation results of the C<sub>3</sub>/C<sub>2</sub> product selectivity on different catalysts show a good agreement with experimental ones (right). (c) Computed concentration and distribution of species. CO<sub>2</sub>, C<sub>1</sub>, C<sub>2</sub>, and C<sub>3</sub> concentrations on the multihollow structure. (Figure adapted with permissions from References 96 and 94. Copyright 2020 American Chemical Society and 2018 Springer Nature)

**BOX 1**

Mechanisms beyond energetics revealed by multiscale kinetics modeling.

## 4 | CONCLUSION AND FUTURE PERSPECTIVE

In past decades, we have witnessed a tendency that theoretical and computational chemistry focused more and more on the energetic. However, there were also some experiments suggested that others such as mass transport could also be crucial for complex systems where chemical reactions are coupled with kinetics. We reviewed in this paper some recent progress of mechanisms beyond energetics revealed by multiscale kinetic modeling in epitaxial growth of 2D materials and electrocatalysis on nanocatalysts. As the rapid development of experimental techniques, there will be many new interesting findings observed in similar complex chemical systems. Due to the complexity of involved multiple scales, it is a great opportunity for the development of multiscale modeling and calculation methods. Generally, future studies may follow three steps. First, establishing a system-dependent multiscale method to understand a special experimental observation in a complex chemical system of particular importance. Then, the established method may be extended to similar systems to verify its application as well as the revealed mechanism. The validated method and mechanism in return provide solid theoretical basis for rational design of complex chemical systems with desired functions in experiments. Technically, there are two major issues need to be addressed to establish multiscale modeling and calculation method. The first one is how to fast identify the most relevant freedoms for multiscale modeling of the systems. So far, success of the established model can only rely on the experience of the researchers. Some general ideas adopted in statistical-mechanics-based methods revealing kinetics of other complex chemical systems, such as kinetic network models for self-assembly and protein dynamics,<sup>1,2</sup> may be helpful for addressing such an issue. The second one is how to integrate calculation methods at different scales together to provide quantitatively reliable calculations with sufficient efficiency, requiring not only well designed algorithms, but also how fine the multiscale models is when we address the first issue. We believe that multiscale modeling and calculation will play an important role in future studies of complex chemical systems where reactions meet kinetics.

### CONFLICT OF INTEREST

The authors have declared no conflict of interest for this article.

### AUTHOR CONTRIBUTIONS

**Huijun Jiang:** Funding acquisition; investigation; visualization; writing-original draft; writing-review and editing.

**Zhonghuai Hou:** Funding acquisition; supervision; writing-review and editing.

### DATA AVAILABILITY STATEMENT

Data sharing is not applicable to this article as no new data were created or analyzed in this study.

### ORCID

Zhonghuai Hou  <https://orcid.org/0000-0003-1241-7041>

### RELATED WIREs ARTICLES

[Constructing Markov State Models to elucidate the functional conformational changes of complex biomolecules](#)  
[Multiscale simulation on thermal stability of supported metal nanocatalysts](#)

### REFERENCES

1. Wang W, Cao S, Zhu L, Huang X. Constructing Markov state models to elucidate the functional conformational changes of complex biomolecules. *Wiley Interdiscip Rev Comput Mol Sci.* 2018;8(1):e1343.
2. Zeng X, Zhu L, Zheng X, Cecchini M, Huang X. Harnessing complexity in molecular self-assembly using computer simulations. *Phys Chem Chem Phys.* 2018;20(10):6767–76.
3. Walpole J, Papin JA, Peirce SM. Multiscale computational models of complex biological systems. *Annu Rev Biomed Eng.* 2013;15:137–54.

4. Smith CP, White HS. Theory of the voltammetric response of electrodes of submicron dimensions. Violation of electroneutrality in the presence of excess supporting electrolyte. *Anal Chem.* 1993;65(23):3343–53.
5. Chen S, Kucernak A. The voltammetric response of nanometer-sized carbon electrodes. *J Phys Chem B.* 2002;106(36):9396–404.
6. He R, Chen S, Yang F, Wu B. Dynamic diffuse double-layer model for the electrochemistry of nanometer-sized electrodes. *J Phys Chem B.* 2006;110(7):3262–70.
7. Morris RB, Franta DJ, White HS. Electrochemistry at pt band electrodes of width approaching molecular dimensions. Breakdown of transport equations at very small electrodes. *J Phys Chem.* 1987;91:3559–64.
8. Watkins JJ, White HS. The role of the electrical double layer and ion pairing on the electrochemical oxidation of hexachloroiridate(iii) at pt electrodes of nanometer dimensions. *Langmuir.* 2004;20:5474–83.
9. Streeter I, Baron R, Compton RG. Voltammetry at nanoparticle and microparticle modified electrodes theory and experiment. *J Phys Chem C.* 2007;111(45):17008–14.
10. Streeter I, Compton RG. Diffusion-limited currents to nanoparticles of various shapes supported on an electrode; spheres, hemispheres, and distorted spheres and hemispheres. *J Phys Chem C.* 2007;111:18049–54.
11. Chen S, Liu Y. Electrochemistry at nanometer-sized electrodes. *Phys Chem Chem Phys.* 2014;16(2):635–52.
12. Lin C, Compton RG. Size effects in nanoparticle catalysis at nanoparticle modified electrodes: the interplay of diffusion and chemical reactions. *J Phys Chem C.* 2017;121(5):2521–8.
13. Lin C, Compton RG. Understanding mass transport influenced electrocatalysis at the nanoscale via numerical simulation. *Curr Opin Electrochem.* 2019;14:186–99.
14. Liu M, Pang Y, Zhang B, de Luna P, Voznyy O, Xu J, et al. Enhanced electrocatalytic CO<sub>2</sub> reduction via field-induced reagent concentration. *Nature.* 2016;537(7620):382–6.
15. Jiang H, Hou Z, Luo Y. Unraveling the mechanism for the sharp-tip enhanced electrocatalytic carbon dioxide reduction: the kinetics decide. *Angew Chem Int Ed Engl.* 2017;56(49):15617–21.
16. Tetlow H, Posthuma de Boer J, Ford IJ, Vvedensky DD, Coraux J, Kantorovich L. Growth of epitaxial graphene: theory and experiment. *Phys Rep.* 2014;542(3):195–295.
17. Parr RG. Density functional theory of atoms and molecules. *Horizons of quantum chemistry.* Dordrecht: Springer; 1980. p. 5–15.
18. Dreizler RM, Gross EK. *Density functional theory: an approach to the quantum many-body problem.* Berlin Heidelberg: Springer Science & Business Media; 2012.
19. Koch W, Holthausen MC. *A chemist's guide to density functional theory.* Weinheim: John Wiley & Sons; 2015.
20. Martin RM. *Electronic structure: basic theory and practical methods.* Cambridge: Cambridge University Press; 2020.
21. Andersen HC. Molecular dynamics simulations at constant pressure and/or temperature. *J Chem Phys.* 1980;72(4):2384–93.
22. Binder K. *Monte carlo and molecular dynamics simulations in polymer science.* New York: Oxford University Press; 1995.
23. Gubbins KE, Quirke N. *Molecular simulation and industrial applications: methods, examples, and prospects.* Vol 1. Amsterdam: Gordon & Breach; 1996.
24. Frenkel D, Smit B. *Understanding molecular simulation: from algorithms to applications.* San Diego: Academic Press; 2001.
25. Allen MP, Tildesley DJ. *Computer simulation of liquids.* Oxford: Oxford University Press; 2017.
26. Voter AF. Introduction to the kinetic Monte Carlo method. *Radiation effects in solids.* Dordrecht: Springer; 2007. p. 1–23.
27. Gillespie DT. Stochastic simulation of chemical kinetics. *Annu Rev Phys Chem.* 2007;58:35–55.
28. Gillespie DT, Hellander A, Petzold LR. Perspective: stochastic algorithms for chemical kinetics. *J Chem Phys.* 2013;138(17):05B201\_1.
29. Chatterjee A, Vlachos DG. An overview of spatial microscopic and accelerated kinetic Monte Carlo methods. *J Comp-aided Mater Design.* 2007;14(2):253–308.
30. Battaile CC. The kinetic Monte Carlo method: foundation, implementation, and application. *Comput Methods Appl Mech Eng.* 2008;197(41–42):3386–98.
31. Eringen AC, Ingram JD. A continuum theory of chemically reacting media—i. *Int J Eng Sci.* 1965;3(2):197–212.
32. Ingram JD, Eringen AC. A continuum theory of chemically reacting media—ii constitutive equations of reacting fluid mixtures. *Int J Eng Sci.* 1967;5(4):289–322.
33. Lichtner PC. Continuum model for simultaneous chemical reactions and mass transport in hydrothermal systems. *Geochim Cosmochim Acta.* 1985;49(3):779–800.
34. Grindrod P. *The theory and applications of reaction-diffusion equations: patterns and waves.* New York: Clarendon Press; 1996.
35. Mennucci B, Cammi R. *Continuum solvation models in chemical physics: from theory to applications.* Chichester: John Wiley & Sons; 2007.
36. Fife PC. *Mathematical aspects of reacting and diffusing systems.* Berlin Heidelberg: Springer-Verlag; 1979.
37. Karplus M, McCammon JA. Molecular dynamics simulations of biomolecules. *Nat Struct Biol.* 2002;9(9):646–52.
38. Van Duin AC, Dasgupta S, Lorant F, Goddard WA. Reaxff: a reactive force field for hydrocarbons. *Chem A Eur J.* 2001;105(41):9396–409.
39. Liang T, Shin YK, Cheng Y-T, Yilmaz DE, Vishnu KG, Verners O, et al. Reactive potentials for advanced atomistic simulations. *Annu Rev Mat Res.* 2013;43:109–29.
40. Honig B, Karplus M. Implications of torsional potential of retinal isomers for visual excitation. *Nature.* 1971;229(5286):558–60.
41. Warshel A, Karplus M. Calculation of ground and excited state potential surfaces of conjugated molecules. I. Formulation and parameterization. *J Am Chem Soc.* 1972;94(16):5612–25.

42. Pariser R, Parr RG. A semi-empirical theory of the electronic spectra and electronic structure of complex unsaturated molecules. I. *J Chem Phys.* 1953;21(3):466–71.
43. Pople JA. Electron interaction in unsaturated hydrocarbons. *Trans Faraday Soc.* 1953;49:1375–85.
44. Warshel A, Levitt M. Theoretical studies of enzymic reactions: dielectric, electrostatic and steric stabilization of the carbonium ion in the reaction of lysozyme. *J Mol Biol.* 1976;103(2):227–49.
45. Levitt M, Warshel A. Computer simulation of protein folding. *Nature.* 1975;253(5494):694–8.
46. Bortz AB, Kalos MH, Lebowitz JL. A new algorithm for Monte Carlo simulation of ising spin systems. *J Comput Phys.* 1975;17(1):10–8.
47. Fichtorn KA, Weinberg WH. Theoretical foundations of dynamical Monte Carlo simulations. *J Chem Phys.* 1991;95(2):1090–6.
48. Serebrinsky SA. Physical time scale in kinetic Monte Carlo simulations of continuous-time markov chains. *Phys Rev E.* 2011;83(3):037701.
49. Gillespie DT. Exact stochastic simulation of coupled chemical reactions. *J Phys Chem.* 1977;81(25):2340–61.
50. Gillespie DT. A general method for numerically simulating the stochastic time evolution of coupled chemical reactions. *J Comput Phys.* 1976;22(4):403–34.
51. Kolmogorov A, Petrovskii I, Piskunov N. Study of a diffusion equation that is related to the growth of a quality of matter, and its application to a biological problem. *Byul Mosk Gos Univ Ser A Mat Mekh.* 1937;1(1):26.
52. Sutter PW, Flege J-I, Sutter EA. Epitaxial graphene on ruthenium. *Nat Mater.* 2008;7(5):406–11.
53. Kim KS, Zhao Y, Jang H, Lee SY, Kim JM, Kim KS, et al. Large-scale pattern growth of graphene films for stretchable transparent electrodes. *Nature.* 2009;457(7230):706–10.
54. Li X, Cai W, An J, Kim S, Nah J, Yang D, et al. Large-area synthesis of high-quality and uniform graphene films on copper foils. *Science.* 2009;324(5932):1312–4.
55. Loginova E, Bartelt NC, Feibelman PJ, McCarty KF. Evidence for graphene growth by C cluster attachment. *New J Phys.* 2008;10(9):093026.
56. Loginova E, Bartelt N, Feibelman P, McCarty K. Factors influencing graphene growth on metal surfaces. *New J Phys.* 2009;11(6):063046.
57. Wu P, Jiang H, Zhang W, Li Z, Hou Z, Yang J. Lattice mismatch induced nonlinear growth of graphene. *J Am Chem Soc.* 2012;134(13):6045–51.
58. Jiang H, Wu P, Hou Z, Li Z, Yang J. Orientation-sensitive nonlinear growth of graphene: an epitaxial growth mechanism determined by geometry. *Phys Rev B.* 2013;88(5):054304.
59. Dong G, Frenken JW. Kinetics of graphene formation on rh (111) investigated by in situ scanning tunneling microscopy. *ACS Nano.* 2013;7(8):7028–33.
60. Jiang H, Hou Z. Large-scale epitaxial growth kinetics of graphene: a kinetic Monte Carlo study. *J Chem Phys.* 2015;143(8):084109.
61. Van Der Zande AM, Huang PY, Chenet DA, Berkelbach TC, You Y, Lee G-H, et al. Grains and grain boundaries in highly crystalline monolayer molybdenum disulphide. *Nat Mater.* 2013;12(6):554–61.
62. Chen C, Feng Z, Feng Y, Yue Y, Qin C, Zhang D, et al. Large-scale synthesis of a uniform film of bilayer MoS<sub>2</sub> on graphene for 2d heterostructure phototransistors. *ACS Appl Mater Interfaces.* 2016;8(29):19004–11.
63. Sledzinska M, Quey R, Mortazavi B, Graczykowski B, Placidi M, Saleta Reig D, et al. Record low thermal conductivity of polycrystalline MoS<sub>2</sub> films: tuning the thermal conductivity by grain orientation. *ACS Appl Mater Interfaces.* 2017;9(43):37905–11.
64. Sangwan VK, Lee H-S, Bergeron H, Balla I, Beck ME, Chen K-S, et al. Multi-terminal memtransistors from polycrystalline monolayer molybdenum disulfide. *Nature.* 2018;554(7693):500–4.
65. Yazyev OV, Louie SG. Electronic transport in polycrystalline graphene. *Nat Mater.* 2010;9(10):806–9.
66. Bagri A, Kim S-P, Ruoff RS, Shenoy VB. Thermal transport across twin grain boundaries in polycrystalline graphene from non-equilibrium molecular dynamics simulations. *Nano Lett.* 2011;11(9):3917–21.
67. Chen S, Gao J, Srinivasan BM, Zhang G, Yang M, Chai J, et al. Revealing the grain boundary formation mechanism and kinetics during polycrystalline MoS<sub>2</sub> growth. *ACS Appl Mater Interfaces.* 2019;11(49):46090–100.
68. Cheng J, Jiang T, Ji Q, Zhang Y, Li Z, Shan Y, et al. Kinetic nature of grain boundary formation in as-grown MoS<sub>2</sub> monolayers. *Adv Mater.* 2015;27(27):4069–74.
69. Park S, Kim MS, Kim H, Lee J, Han GH, Jung J, et al. Spectroscopic visualization of grain boundaries of monolayer molybdenum disulfide by stacking bilayers. *ACS Nano.* 2015;9(11):11042–8.
70. Duan X, Wang C, Pan A, Yu R, Duan X. Two-dimensional transition metal dichalcogenides as atomically thin semiconductors: opportunities and challenges. *Chem Soc Rev.* 2015;44(24):8859–76.
71. Hsu Y-T, Vaezi A, Fischer MH, Kim E-A. Topological superconductivity in monolayer transition metal dichalcogenides. *Nat Commun.* 2017;8(1):1–6.
72. Baugher BW, Churchill HO, Yang Y, Jarillo-Herrero P. Optoelectronic devices based on electrically tunable p–n diodes in a monolayer dichalcogenide. *Nat Nanotechnol.* 2014;9(4):262–7.
73. Zhou J, Lin J, Huang X, Zhou Y, Chen Y, Xia J, et al. A library of atomically thin metal chalcogenides. *Nature.* 2018;556(7701):355–9.
74. Chen W, Zhao J, Zhang J, Gu L, Yang Z, Li X, et al. Oxygen-assisted chemical vapor deposition growth of large single-crystal and high-quality monolayer MoS<sub>2</sub>. *J Am Chem Soc.* 2015;137(50):15632–5.
75. Chowdhury T, Kim J, Sadler EC, Li C, Lee SW, Jo K, et al. Substrate-directed synthesis of MoS<sub>2</sub> nanocrystals with tunable dimensionality and optical properties. *Nat Nanotechnol.* 2020;15(1):29–34.

76. Ma Z, Wang S, Deng Q, Hou Z, Zhou X, Li X, et al. Epitaxial growth of rectangle shape MoS<sub>2</sub> with highly aligned orientation on twofold symmetry a-plane sapphire. *Small*. 2020;16(16):2000596.
77. Duan Z, Chen T, Shi J, Li J, Song K, Zhang C, et al. Space-confined and substrate-directed synthesis of transition-metal dichalcogenide nanostructures with tunable dimensionality. *Sci Bull*. 2020;65:1013–21.
78. Wu L, Yang W, Wang G. Mechanism of substrate-induced anisotropic growth of monolayer WS<sub>2</sub> by kinetic Monte Carlo simulations. *npj 2D Mater Appl*. 2019;3(1):1–7.
79. Wang Y, Laborda E, Ward KR, Tschulik K, Compton RG. A kinetic study of oxygen reduction reaction and characterization on electrodeposited gold nanoparticles of diameter between 17 nm and 40 nm in 0.5 M sulfuric acid. *Nanoscale*. 2013;5(20):9699–708.
80. Zhou YG, Rees NV, Compton RG. Electrochemistry of nickel nanoparticles is controlled by surface oxide layers. *Phys Chem Chem Phys*. 2013;15(3):761–3.
81. Chen QX, Liu YH, Qi XZ, Liu JW, Jiang HJ, Wang JL, et al. Ordered nanostructure enhances electrocatalytic performance by directional micro-electric field. *J Am Chem Soc*. 2019;141(27):10729–35.
82. Li M, Garg S, Chang X, Ge L, Li L, Konarova M, et al. Toward excellence of transition metal-based catalysts for CO<sub>2</sub> electrochemical reduction: an overview of strategies and rationales. *Small Methods*. 2020;4(7):2000033.
83. Gao FY, Hu SJ, Zhang XL, Zheng YR, Wang HJ, Niu ZZ, et al. High-curvature transition-metal chalcogenide nanostructures with a pronounced proximity effect enable fast and selective CO<sub>2</sub> electroreduction. *Angew Chem*. 2020;132(22):8784–90.
84. Zhang F, Chen C, Yan S, Zhong J, Zhang B, Cheng Z. Cu@bi nanocone induced efficient reduction of CO<sub>2</sub> to formate with high current densities. *Appl Catal Gen*. 2020;598:117545.
85. Chen C, Pang Y, Zhang F, Zhong J, Zhang B, Cheng Z. Sharp Cu@Sn nanocones on Cu foam for highly selective and efficient electrochemical reduction of CO<sub>2</sub> to formate. *J Mater Chem A*. 2018;6(40):19621–30.
86. Zhao J, Xue S, Barber J, Zhou Y, Meng J, Ke X. An overview of Cu-based heterogeneous electrocatalysts for CO<sub>2</sub> reduction. *J Mater Chem A*. 2020;8(9):4700–34.
87. Li YH, Liu PF, Li C, Yang HG. Sharp-tipped zinc nanowires as an efficient electrocatalyst for carbon dioxide reduction. *Chemistry—A Eur J*. 2018;24(58):15486–90.
88. An P, Wei L, Li H, Yang B, Liu K, Fu J, et al. Enhancing CO<sub>2</sub> reduction by suppressing hydrogen evolution with polytetrafluoroethylene protected copper nanoneedles. *J Mater Chem A*. 2020;8:15936–41.
89. Ni W, Xue Y, Zang X, Li C, Wang H, Yang Z, et al. Fluorine doped cage-like carbon electrocatalyst: an insight into the structure-enhanced co selectivity for CO<sub>2</sub> reduction at high overpotential. *ACS Nano*. 2020;14(2):2014–23.
90. Ye S, Fan G, Xu J, Yang L, Li F. Nickel-nitrogen-modified porous carbon/carbon nanotube hybrid with necklace-like geometry: an efficient and durable electrocatalyst for selective reduction of CO<sub>2</sub> to CO in a wide negative potential region. *Electrochim Acta*. 2020;334:135583.
91. Jia C, Zhang Y, Wang X, Zhong W, Prezhdo OV, Luo Y, et al. Sharp-tip enhanced catalytic CO oxidation by atomically dispersed Pt<sub>1</sub>/Pt<sub>2</sub> on raised graphene oxide platform. *J Mater Chem A*. 2020;8:12485–94.
92. Liu D, Li X, Chen S, Yan H, Wang C, Wu C, et al. Atomically dispersed platinum supported on curved carbon supports for efficient electrocatalytic hydrogen evolution. *Nat Energy*. 2019;4(6):512–8.
93. Yang KD, Ko WR, Lee JH, Kim SJ, Lee H, Lee MH, et al. Morphology-directed selective production of ethylene or ethane from CO<sub>2</sub> on a Cu mesopore electrode. *Angew Chem Int Ed Engl*. 2017;56(3):796–800.
94. Yang PP, Zhang XL, Gao FY, Zheng YR, Niu ZZ, Yu X, et al. Protecting copper oxidation state via intermediate confinement for selective CO<sub>2</sub> electroreduction to C<sub>2</sub>+ fuels. *J Am Chem Soc*. 2020;142(13):6400–8.
95. Kortlever R, Shen J, Schouten KJ, Calle-Vallejo F, Koper MT. Catalysts and reaction pathways for the electrochemical reduction of carbon dioxide. *J Phys Chem Lett*. 2015;6(20):4073–82.
96. Zhuang T-T, Pang Y, Liang Z-Q, Wang Z, Li Y, Tan C-S, et al. Copper nanocavities confine intermediates for efficient electrosynthesis of C<sub>3</sub> alcohol fuels from carbon monoxide. *Nature Catal*. 2018;1(12):946–51.
97. Sandberg RB, Montoya JH, Chan K, Nørskov JK. Co-Co coupling on Cu facets: coverage, strain and field effects. *Surf Sci*. 2016;654:56–62.

**How to cite this article:** Jiang H, Hou Z. Mechanisms beyond energetics revealed by multiscale kinetic modeling of 2D-material growth and nanocatalysis. *WIREs Comput Mol Sci*. 2021;e1524. <https://doi.org/10.1002/wcms.1524>